Journal of Alloys and Compounds 505 (2010) 818–823

Contents lists available at ScienceDirect

Journal of Alloys and Compounds

journal homepage: www.elsevier.com/locate/jallcom

Synthesis and characterization of manganese-doped zinc orthosilicate phosphor powders

Mu-Tsun Tsai*, Yu-Feng Lu, Yen-Kai Wang

Department of Materials Science and Engineering, National Formosa University, P.O. Box 385 Douliu, Yunlin 640, Taiwan

ARTICLE INFO

Article history:
Received 10 January 2010
Received in revised form 17 June 2010
Accepted 24 June 2010
Available online 21 July 2010

Keywords:
Nanostructured materials
Phosphors
Zn_2SiO_4:Mn
Sol–gel
Luminescence

ABSTRACT

Homogeneous and nanocrystalline manganese-doped zinc orthosilicate (Zn_2SiO_4:Mn) phosphor powders were prepared using a sol–gel process by controlling the hydrolysis of silicon alkoxide and zinc chloride precursors. The Mn dopant content influenced the gelation rate, homogeneity, degree of agglomeration, and luminescence of powders. Mn-doped xerogel powders were amorphous and crystallized into pure willemite (α-Zn_2SiO_4) structure when heated to 600 °C. After heating at 800–1000 °C, the crystallite sizes of $Zn_{2-x}Mn_xSiO_4$ phosphor powders were around 15–32 nm at an Mn doping level of x = 0.2–20 mol%. The resulting powder phosphors exhibited prominent photoluminescence emission peaks centered at 520–529 nm, depending on the doping content. The intensity of the green emission was strongly related to the dopant content and improved crystallinity. Furthermore, reducing the specific surface area and pore volume further enhanced the luminous efficiency of willemite powders. The sol–gel transition, crystallinity, microstructure, and luminescent property of phosphor powders were investigated.

1. Introduction

Manganese-doped zinc orthosilicate (α-Zn_2SiO_4, willemite) has been widely used as a green phosphor in cathode ray tubes and lamps, and more recently in flat panel displays, owing to its high luminescence efficiency, high saturated color, and chemical stability [1–3]. Since Zn^{2+} and Mn^{2+} ions have similar oxidation states and radii, the substitution of Zn^{2+} ions with Mn^{2+} yields excellent green phosphors. The green emission is attributed to a d-orbital electron transition of the Mn^{2+} ions [4]. Zn_2SiO_4:Mn powder phosphor is conventionally synthesized by the solid-state reaction method, which suffers from several limitations, such as a high processing temperature of over 1000 °C, inhomogeneous distribution of activator ions, contamination of impurities, and phase segregation [3,5].

Recently, the sol–gel process has been studied and verified to have several advantages over the conventional method, including lower temperature process, better homogeneity, and higher emission efficiency of the powder phosphors [6–11]. However, most of the work concerning the sol–gel synthesis of pure or Mn-doped zinc silicate has normally used zinc acetate or zinc nitrate as the starting chemical for Zn. Not only are ZnO and/or β-Zn_2SiO_4 second phases present, but also the willemite derived from the previous sol–gel processes are usually crystallized by heating at temperatures of above 800 °C. Zinc silicate exists in three structural polymorphs, i.e. α-, β- and γ-Zn_2SiO_4 [12]. The latter two meta-stable phases transform to α-phase at high temperature. The luminescent property of phosphors depends greatly on the crystal structure of host lattice. Consequently, the luminescence from β-Zn_2SiO_4:Mn phosphors is in the yellow region and has a much longer decay time than that of Mn-doped willemite in the green region [11]. Therefore, synthesizing a pure Mn-doped willemite phase as the reliable green component to be used in the display devices is very important.

Sol–gel processing has been extensively studied for use in preparing nanostructured ceramics and glasses. The property of gel-derived products depends strongly on the precursor used [13]. Also, quantum confinement in nanocrystalline phosphors can enhance luminous efficiency, as has been observed in several powder phosphors [14–16]. Hence, preparing homogeneous and nanostructured Mn-doped willemite powder phosphor by the sol–gel method with a suitably chosen molecular precursor is very significant.

In this work, undoped and Mn-doped zinc orthosilicate powders were prepared by the sol–gel process using zinc chloride-based precursors. The sol–gel transition, crystallization process, and photoluminescence (PL) property of processed powders are investigated. The dependence of luminescence on powder texture is also examined in terms of specific surface area and pore volume.

2. Experimental

2.1. Synthesis

Zinc chloride ($ZnCl_2$), tetraethylorthosilicate ($Si(OC_2H_5)_4$; TEOS), and manganese chloride ($MnCl_2{\cdot}4H_2O$) were used as sources of zinc, silicon, and manganese, respectively. Tetraethylorthosilicate was firstly partially hydrolyzed at a molar ratio of TEOS:water:HCl = 1:1:0.5:0.01. Willemite precursor sols were prepared by dis-

* Corresponding author. Tel.: +886 5 5320731; fax: +886 5 6361981.
E-mail address: mttsai@ms23.hinet.net (M.-T. Tsai).

0925-8388/$ – see front matter © 2010 Elsevier B.V. All rights reserved.
doi:10.1016/j.jallcom.2010.06.147

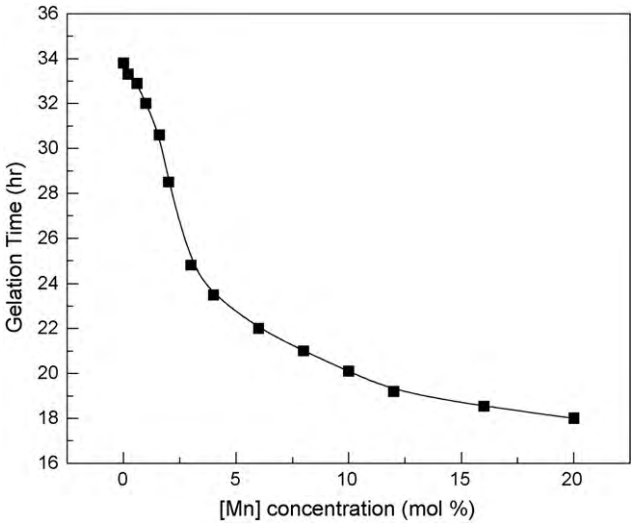

Fig. 1. The influence of manganese concentration on the gelation time of precursor sols.

solving zinc chloride in the pre-hydrolyzed TEOS solution with a molar ratio of Zn:Si of 2:1. The mixed solution was stirred and refluxed at room temperature, and then the desired amount of manganese chloride and a small content of deionized water (0.5 molar ratio to Si) were added for doping and hydrolysis. The obtained transparent sols were then kept open at ambient temperature until gelation. The xerogel powders were prepared by drying the gels at 100 °C in an oven and then grinding them, subsequently firing the powders for 2 h at various temperatures from 500 to 1000 °C in a reducing atmosphere. The amount of manganese was varied with an Mn^{2+}:Zn_2SiO_4 molar ratio of 0.2–20 mol% to investigate the dependences of crystallization and luminescence on doping. To examine the influence of powder texture on the luminescence, some of the phosphor powders were heated for 2–10 h at 1000 °C.

2.2. Characterization

The viscosity of the solutions was measured throughout the gelation period at 25 °C using a Brookfield viscometer and a UL adaptor. The gelation time was measured as the time at which the maximum viscosity of the sol was reached under a constant shear rate. The crystalline phase of the processed samples was examined by powder X-ray diffractometry (XRD; Rigaku D/MAX-III) with Ni-filtered Cu Kα radiation. Differential thermal analysis/thermogravimetry (Setaram DTA/TG) were performed in flowing air at a heating rate of 10 °C min^{-1}. The specific surface area and pore volume were determined from nitrogen adsorption–desorption isotherms obtained at 77 K (liquid N_2) using an automatic instrument (ASAP2020, Micromeritics). Prior to measurements, samples were degassed at 300 °C for 3–4 h and 10^{-2} Torr. The morphology of the powder was observed by field-emission scanning electron microscopy (FE-SEM; JEOL JSM-6700F). The excitation and emission spectra were recorded at room temperature on a Hitachi F4500 fluorescence spectrometer with a 150 W xenon lamp as the excitation source.

3. Results and discussion

All of the obtained precursor gels were transparent after gelation, irrespective of the level of manganese doping. The doping concentration, however, influenced the gelation rate. Fig. 1 reveals that the gelation time is a function of manganese concentration. The gelation time declined markedly as the manganese content increased, reflecting the different degrees of sol–gel transition among those sols. Since all of the sol samples herein were kept open to the ambient atmosphere during the gelation process, the drop in gelation time may have been caused by the evaporation and hydrolysis–condensation reaction of sols [17]. Notably, the dopant precursor contained much water of hydration. Increasing the amount of dopant would have introduced more water into the precursor sols, promoting hydrolytic polycondensation and therefore shortening the gelation time. Additionally, all of the investigated sols were transparent during gelation, indicating that homogeneous precursor sols were formed at an Mn doping level of 0–20%.

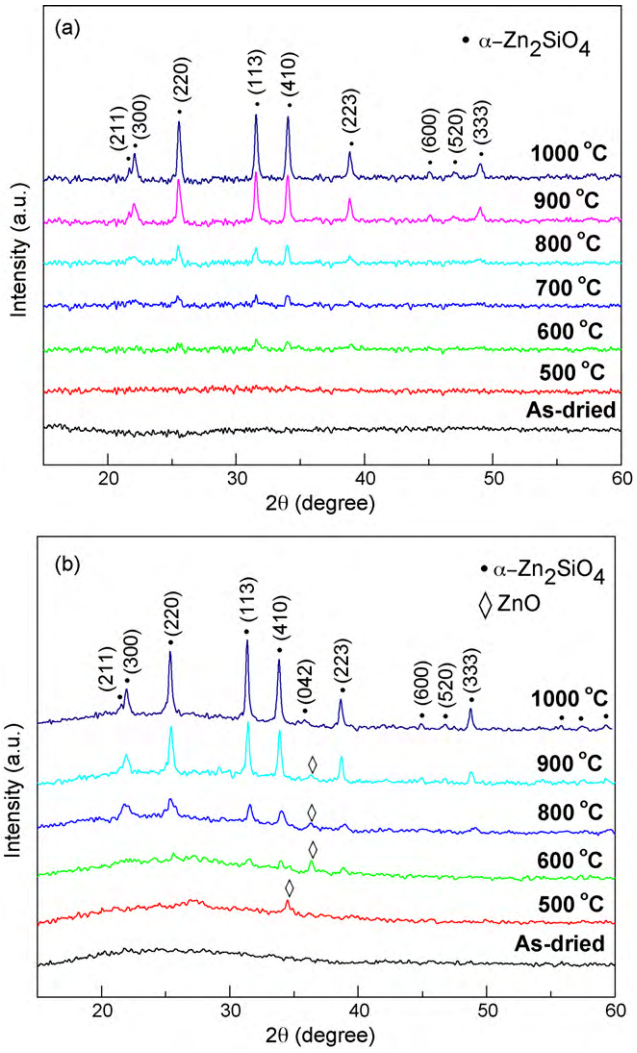

Fig. 2. X-ray diffraction patterns of (a) 6% Mn-doped and (b) 20% Mn-doped Zn_2SiO_4 powders after heat treatment at various temperatures for 2 h.

Fig. 2 compares the XRD patterns of the Mn-doped Zn_2SiO_4 (Mn = 6 and 20%) powder samples following heat treatment at various temperatures for 2 h. The sample with Mn = 6% (Fig. 2a) remained amorphous after calcination up to 500 °C. Some weak diffraction peaks appeared following calcining at 600 °C, moreover, the peaks and intensity increased with the firing temperature up to 1000 °C. All of the diffraction peaks matched the standard pattern for rhombohedral willemite phase (α-Zn_2SiO_4, JCPDS card no. 37-1485). No trace of ZnO or any other crystalline phase, such as β-Zn_2SiO_4 or manganese oxide, was detected. The undoped samples and those doped with an Mn content less than 20% had similar features. Although the 20% Mn-doped sample (Fig. 2b) yields similar XRD results, but minor ZnO (1 0 1) and (0 0 2) peaks (JCPDS card no. 36-1451) were found following calcination at 900 °C and below. After further heating at 1000 °C, willemite was the dominant phase. Upon heating at 800–1000 °C, the average crystallite sizes were around 15–30 nm for Mn = 6% and 16–32 nm for Mn = 20% powder phosphors, as estimated from the (2 2 0), (1 1 3), and (4 1 0) reflections using Scherer's equation.

Fig. 2 also reveals that crystallinity increased significantly with calcination temperature from 800 to 1000 °C. Similar feature was also observed when increased the duration of calcination from 2 to 10 h at 1000 °C. The results show that the crystallinity of willemite in this work depends mainly on the heating temperature and the

heating time. In contrast, the Mn doping level had no significant effect on the crystallinity. Both precursor gels had similar transparent appearances. However, a comparison of the XRD results in Fig. 2a and b suggest different degrees of homogeneity in the two gel powders following heating, even though their crystallinities were similar. The sample with a large amount of dopant probably contained more water, promoting gelation and inducing local chemical inhomogeneity, resulting in the formation of the ZnO secondary phase on heating. Similar results were also observed when the starting materials were directly mixed without the prehydrolysis of TEOS, independently of doping content. The fact that the hydrolysis of silicon alkoxide is much slower than that of zinc chloride may explain such chemical heterogeneity of gel powders. In this study, the prehydrolysis of TEOS had a positive effect on the formation of homogeneous willemite gel powders. The dried powders are amorphous to XRD, which inferring that both zinc and silicon ions were uniformly distributed in the xerogel and Si–O–Mg linkages might occur. However, further investigations of their molecular structures are needed. Notably, the Mn had high solubility in willemite gel. Studies are now being undertaken to increase the homogeneity of willemite powders that are doped with high Mn content by closely controlling the amounts of water and various dopant compounds.

On calcining at 800–1000 °C, all of the powders were white, indicating that the manganese ions were in the divalent state [2,18]. XRD examination revealed that single-phase α-Zn_2SiO_4 was formed by the present sol–gel approach with proper doping concentrations, suggesting that the Mn^{2+} ions were well dispersed as substitutes for Zn^{2+} in the zinc silicate host lattice after heating. Accordingly, homogeneous Mn^{2+}-willemite solid solutions (α-$Zn_{2-x}Mn_xSiO_4$ ($0.2 \leq x < 20$ mol%)) were formed, since no trace of MnO_x or any other impurity phase was detected. XRD results also indicated that willemite crystallite began to be formed at temperatures as low as 600 °C. This synthesis temperature is apparently lower than those reported previously for the solid-state reaction [2,6] and sol–gel routes using zinc acetate-based or zinc nitrate-based precursors [6–11], revealing the advantages of this approach.

Fig. 3 displays the TG and DTA curves for Zn_2SiO_4:Mn xerogel powders (Mn = 6 and 20%). Both the DTA curves exhibited sharp endothermic peaks around 120 and 560 °C, corresponding to significant weight losses around 30–200 °C and 420–580 °C in the TG curves of the two samples. This result is attributed mainly to the evaporation and decomposition of water and organic residues, respectively. No significant weight loss occurred above 800 °C. However, DTA curves did not present a well-defined exothermic peak, indicating that crystallization occurred slowly in those samples. According to the XRD results (Fig. 2), the crystallization of willemite began at 600 °C. Hence, the removal of residual organics can be considered to have induced the conversion of amorphous precursor into crystallized willemite in the powder phosphors. Thermal analysis also reveals that the two gel powders have essentially similar thermal reactivities.

Fig. 4 shows SEM photographs of the undoped and Mn-doped powders after heating at 1000 °C for 2 h. The undoped Zn_2SiO_4 powders (Fig. 4a) consisted of granular structures with round morphology, which were slightly agglomerated. The mean primary particle size was found to be around 35 nm, as measured from the scanning electron micrograph. The doped powders (Fig. 4b and c) had similar particle sizes of 30–40 nm for Mn = 6 and 20%, which is close to the crystallite size that was estimated from the XRD results. However, the degree of agglomeration increased with the Mn doping content to 20%, as observed by comparing Fig. 4a with c. Although the doping concentration did not strongly affect the thermal reactivity of powder, a high dopant content influenced the agglomeration state. This effect may be related to the fact that more water was introduced into the sols when more dopant was added, as noted previously. In the sol–gel approach, a higher water

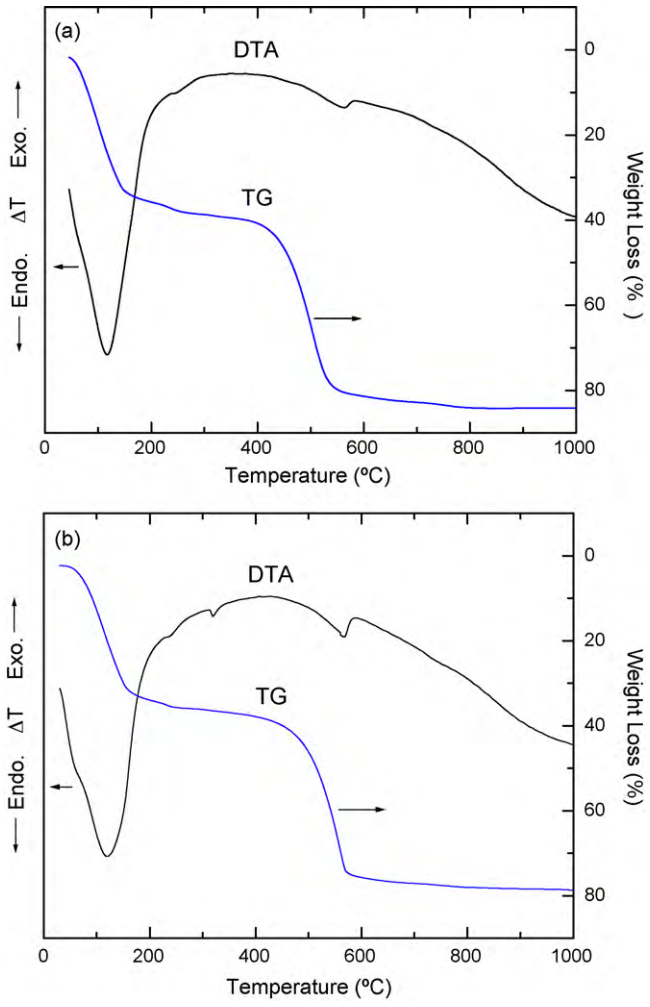

Fig. 3. TG and DTA curves of $Zn_{2-x}Mn_xSiO_4$ gel powders for (a) $x = 6\%$ and (b) $x = 20\%$.

content generally induced the formation of more oxygen bridge bonds among the colloidal particles during gelation [19] and, consequently, greater aggregation of powder. Restated, the high dopant content herein produces the polymeric species with more branched or crossed-linked structures, and therefore a greater degree of agglomeration of the resulting powders.

Fig. 5 presents the excitation spectrum of the 2% Mn-doped Zn_2SiO_4 phosphor powder after calcination at 1000 °C, obtained by monitoring the green emission at 525 nm. The excitation spectrum comprised a strong excitation band from 220 to 300 nm with a maximum at around 275 nm, corresponding to the excitation of the Mn^{2+} charge transfer transition from its ground state $^6A_1(S)$ to the conduction band [2,4]. The maximum intensity and the information at shorter wavelengths can not be detected because of limitations of the instrument used. The other bands associated with the manganese transitions were also observed around 361, 382, 425, 437, and 472 nm, which were assigned to the $^6A_1(S)$–$^4E(^4D)$, $^6A_1(S)$–$^4T_2(^4D)$, $^6A_1(S)$–^4E, $^4A_1(^4G)$, $^6A1(S)$–$^4T_2(^4G)$ and $^6A_1(S)$–$^4T_1(^4G)$ transitions, respectively [4]. According to the Orgel diagram [20], these transitions ascribe to the splitting of the ^4D and ^4G levels of divalent manganese. Similar results have been presented elsewhere [21]. The emission spectra obtained at various excitation wavelengths have a single broad emission peak around 525 nm, as shown in Fig. 6. This peak is associated with the emission of Mn^{2+} in the willemite lattice [2,4,18]. Following excitation by ultraviolet (UV) or visible light, the excited electrons relax to their lowest excited state ($^4T_1$) and then transition from $^4T_1$ to

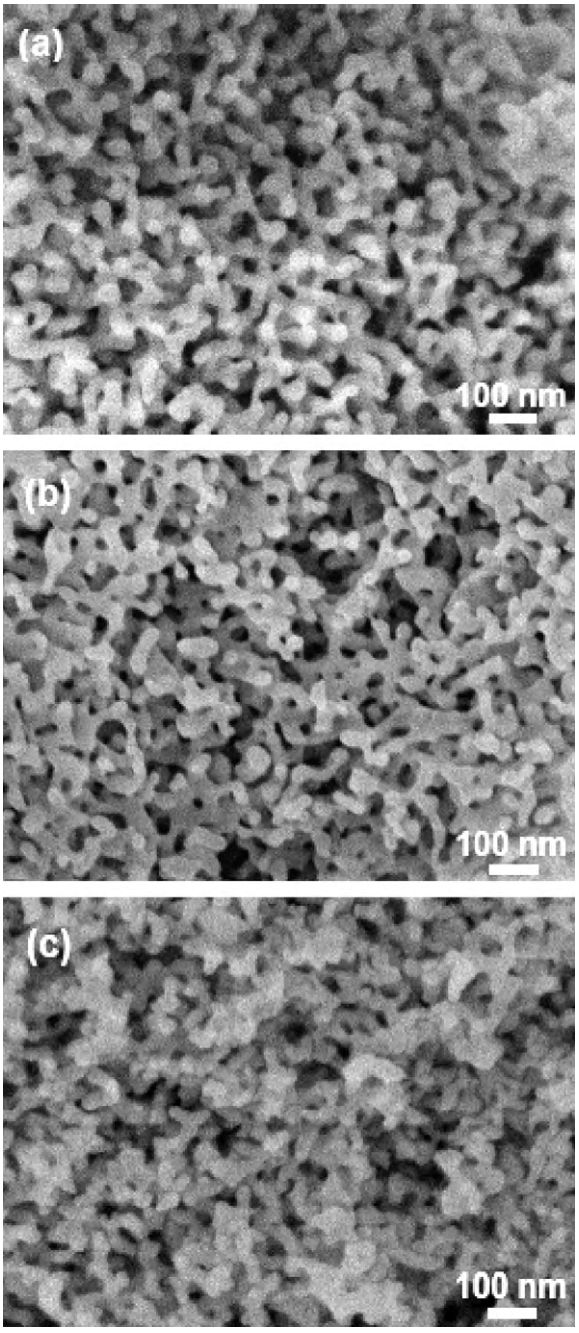

Fig. 4. SEM micrographs of (a) undoped, (b) 6% Mn-doped, and (c) 20% Mn-doped Zn_2SiO_4 powders after firing at 1000 °C.

the ground state ($^6A_1$) of Mn^{2+}, emitting green light. The emission intensity clearly reached its highest value following UV excitation at λ_{ex} = 270 nm.

Fig. 7 shows the emission intensity of 1000 °C heated powders depends on manganese doping content under UV excitation (λ_{ex} = 270 nm). All of the spectra also include an intense green emission band that corresponds to the typical $^4T_1(G_4)$–$^6A_1(^6S)$ transition of Mn^{2+}. This result confirms the formation of an Mn^{2+}-willemite solid solution, α-$Zn_{2-x}Mn_xSiO_4$, in the samples, which is responsible for the saturated green emission under UV excitation. The maximum of the emission band and the peak position varied with respect to doping content. The maximum brightness increased with Mn content up to 6%, but declined significantly as doping increased above 8%. As the Mn concentration increased,

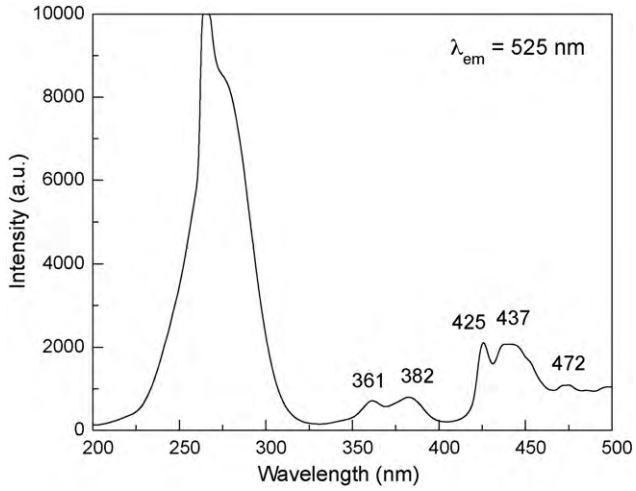

Fig. 5. Excitation spectrum of Mn-doped Zn_2SiO_4 phosphor powder after calcining at 1000 °C, obtained by monitoring the green emission at 525 nm.

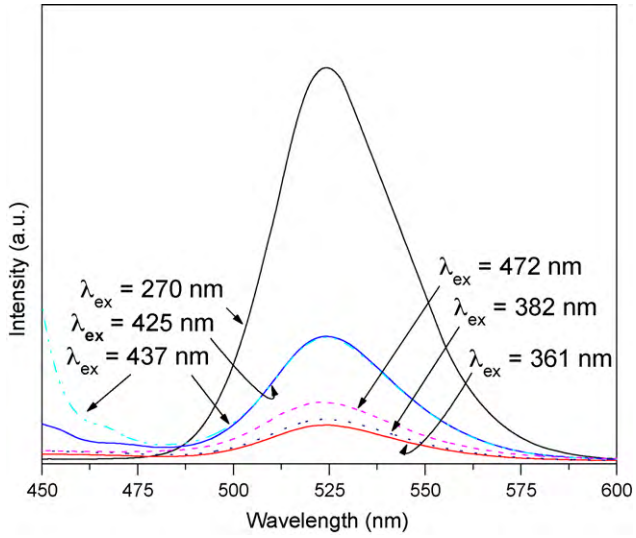

Fig. 6. Emission spectra of Mn-doped Zn_2SiO_4 phosphor powder under various excitation wavelengths, sample is identical to that in Fig. 5.

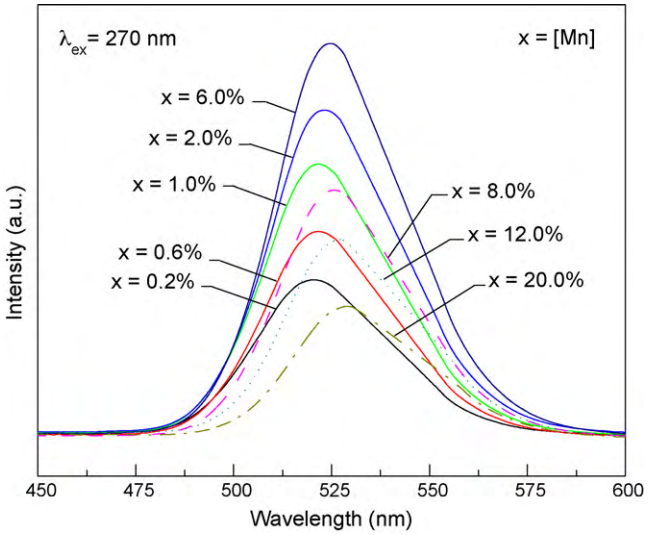

Fig. 7. Emission spectra of 1000 °C heated $Zn_{2-x}Mn_xSiO_4$ powders for various Mn doping concentrations, under UV excitation (λ_{ex} = 270 nm).

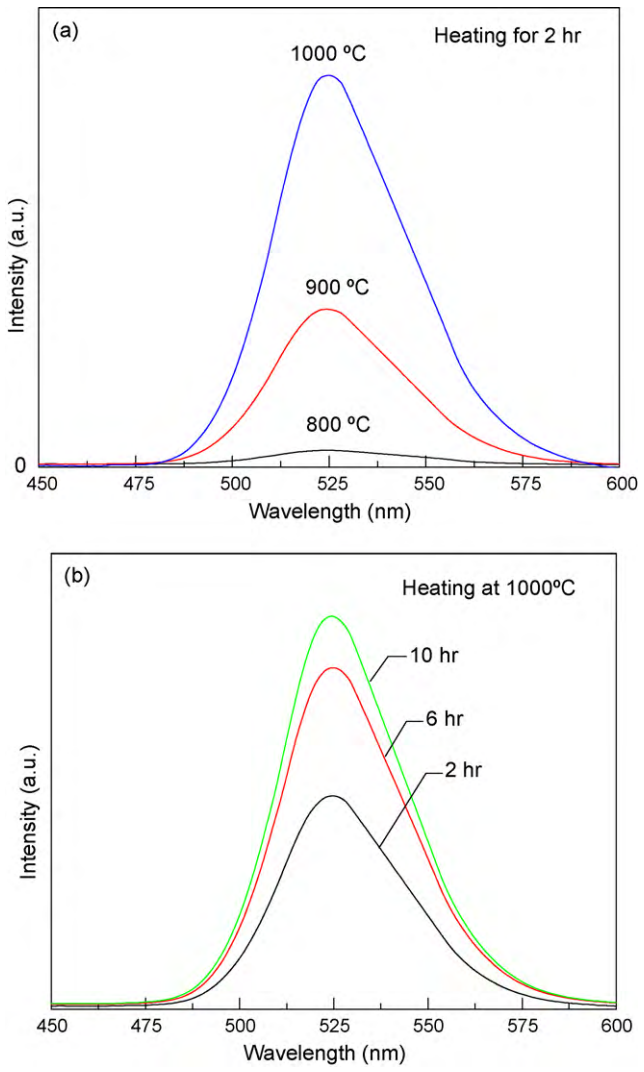

Fig. 8. Emission intensity of 6% Mn-doped Zn_2SiO_4 powders as a function of (a) heating temperature and (b) heating time, under UV excitation (λ_{ex} = 270 nm).

the peak position shifted from 520 to 529 nm. The drop in the intensity of green emission arose mainly from the formation of Mn^{2+} ion pairs by concentration quenching, as suggested by Morrell and Ronda et al. [2,22]. Owing to the formation of the dopant ion pairs or clusters at high concentration, the exchange interaction between Mn^{2+} ions reduced the transition energy, and thus reduced the luminescence efficiency. Exchange interactions between Mn^{2+} ions are also responsible for the red-shift of the emission band [22].

Fig. 8 plots the emission intensity of the 6% Mn-doped powder as a function of heating temperature and heating time. Upon heating to below 800 °C, the luminescent intensity was too weak to be appreciated. It increased markedly with the firing temperatures from 800 to 1000 °C (Fig. 8a). This result, coupled with the XRD patterns (Fig. 2a), reveals that an increase in crystallinity was responsible for the increase in intensity of luminescence. Additionally the heating time strongly affected the brightness of emission, as shown in Fig. 8b. On heating at 1000 °C, the emission intensity of powders increased with duration from 2 to 10 h. This result can also be attributed to the increase in crystallinity, as mentioned previously and possibly, also to the texture of the powder, which was determined from its specific surface area and pore volume. Table 1 presents the results.

Table 1
The influence of heating time on the specific surface area (S_{BET}), pore volume (V_p), and mean pore size (r_p) of 6% Mn-doped Zn_2SiO_4 phosphor powders upon heating at 1000 °C.

Heating time (h)	S_{BET} (m^2/g)	V_p ($\times 10^{-3}$ cm^3/g)	r_p (nm)
2	26.5 (±1)	65.0 (±3)	15.3 (±0.8)
6	20.3 (±1)	45.5 (±2)	14.6 (±0.5)
10	17.0 (±1)	40.3 (±2)	15.8 (±0.5)

The three samples gave nitrogen adsorption isotherms of type IV after heating at 1000 °C for 2–10 h, suggesting that the powders were mesoporous. The mean pore size of the phosphor powders was around 14–16 nm, as listed in Table 1. However, the specific surface area and pore volume of the powder deceased as the heating time increased, meaning that the less of open porosity. Some investigations have suggested that increasing the surface area reduces the luminescence efficiency of conventional phosphor powder probably because of the formation of surface defects [14,16], such as by the absorption of impurities and damage to the surface. Nanocrystalline particles with a higher surface area absorb more impurities. Absorbed water or impurities probably affect the absorption and scattering of the UV light, reducing the luminescence efficiency [14]. In this approach, porosity is also regarded as a surface defect of powders, also affecting the absorption and scattering of the UV light. Presumably, prolongation of heating reduced the porosity and, therefore, the scattering of UV light, enhancing the emission efficiency of powders. Similar results have also been observed from europium-doped phosphor particles that are prepared by spray pyrolysis [23]; the densification of porous Y_2O_3:Eu particles greatly improves luminescence intensity. Restated, luminescence intensity due to the d–d transition of Mn^{2+} in Zn_2SiO_4 nanoparticles herein depends not only on the dopant content and improved crystallinity, but also on the texture of the powder. Reducing the specific surface area and pore volume reduces the open porosity, further improving the luminescent efficiency of powder phosphors.

4. Conclusions

Homogeneous and nanosized manganese-doped willemite ($Zn_{2-x}Mn_xSiO_4$; x = 0.2–20 mol%) powders were successfully prepared by a new sol–gel route. Zinc chloride was identified as the source of Zn in this approach, and is therefore a suitable precursor for the preparation of willemite phosphor. The process described herein has the potential to produce single-phase α-Zn_2SiO_4 at low temperature. The crystallization of willemite began at 600 °C. PL spectra also confirmed the formation of Mn^{2+}-willemite solid solutions. The crystallinity of willemite depended mainly on the heating temperature and the heating time. The dopant content did not markedly affect the crystallinity or thermal reactivity, but did affect the gelation rate and degree of agglomeration of the powders. Upon UV or visible light excitation, the processed phosphor powders revealed the typical green emission of Mn^{2+}. The luminescence intensity is strongly dependent on the dopant content and improvement in crystallinity. Additionally, the luminescence intensity related to the powder texture. Reducing the specific surface area and pore volume further improved the luminescent brightness of powder phosphors.

Acknowledgement

The authors would like to thank the National Science Council of Taiwan for financially supporting this research under Contract No. NSC98-2221-E-150-029.

References

[1] X. Ouyang, A.H. Kitai, T. Xiao, J. Appl. Phys. 79 (1996) 3229–3234.
[2] A. Morell, N. El Khiati, J. Electrochem. Soc. 140 (1993) 2019–2022.
[3] Q.Y. Zhang, K. Pita, C.H. Kam, J. Phys. Chem. Solids 64 (2003) 333–338.
[4] D.T. Palumbo, J. Brown Jr., J. Electrochem. Soc. 117 (1970) 1184–1188.
[5] I.F. Chang, J.W. Brownlow, T.I. Sun, J.S. Wilson, J. Electrochem. Soc. 136 (1989) 3532–3536.
[6] R. Morimo, K. Matae, Mater. Res. Bull. 24 (1989) 175–179.
[7] R. Selomulya, S. Ski, K. Pita, C.H. Kam, Q.Y. Zhang, S. Buddhudu, Mater. Sci. Eng. B 100 (2003) 136–141.
[8] L. Reynaud, C. Brouca-Cabarrecq, A. Mosset, H. Abamdane, Mater. Res. Bull. 31 (1996) 1133–1139.
[9] A. Patra, G.A. Baker, S.N. Baker, J. Lumin. 111 (2005) 105–111.
[10] J. Lin, D.U. Sanger, M. Mennig, K. Barner, Mater. Sci. Eng. B64 (1999) 73–78.
[11] N. Taghavinia, G. Lerondel, H. Makino, A. Yamamoto, T. Yao, Y. Kawazoe, T. Goto, Nanotechnology 12 (2001) 547–551.
[12] E. Ingerson, G.W. Morey, O.F. Tuttle, Am. J. Sci. 246 (1948) 31–40.
[13] C.J. Brinker, G.W. Scherer, Sol–Gel Science, Academic Press, New York, 1990.
[14] B.M. Tissue, Chem. Mater. 10 (1998) 2837–2845.
[15] T.S. Copeland, B.I. Lee, J. Qi, A.K. Elord, J. Luminesc. 97 (2002) 168–173.
[16] G. Wakefield, E. Holland, P.J. Dobson, J.L. Hutchison, Adv. Mater. 13 (2001) 1557–1560.
[17] S. Sakka, K. Kamiya, J. Non-Cryst. Solids 48 (1982) 31–46.
[18] K.S. Sohn, B. Cho, H.D. Park, J. Am. Ceram. Soc. 82 (1999) 2779–2784.
[19] B.E. Yoldas, J. Non-Cryst. Solids 51 (1982) 105–121.
[20] L.E. Orgel, J. Chem. Phys. 23 (1955) 1004–1014.
[21] F. Su, B. Ma, K. Ding, G. Li, S. Wang, W. Chen, A.G. Joly, D.E. McCready, J. Lumin. 116 (2006) 117–126.
[22] C.R. Ronda, T. Amrein, J. Lumin. 69 (1996) 245–248.
[23] K.Y. Jung, K.H. Han, Electrochem. Solid State Lett. 8 (2005) H17–H20.